

Testing machine learning models for heuristic building damage assessment applied to the Italian Database of Observed Damage (DaDO)

Subash Ghimire¹, Philippe Guéguen¹, Adrien Pothon², Danijel Schorlemmer³

¹ISTerre, Université Grenoble Alpes/CNRS/IRD/Université Gustave Eiffel

²AXA Group Risk Management

³German Research Center for Geosciences, Telegrafenberg, Potsdam, Germany,

Correspondence to: Subash Ghimire (subash.ghimire@univ-grenoble-alpes.fr)

Abstract

Assessing or forecasting seismic damage to buildings is an essential issue for earthquake disaster management. In this study, we explore the efficacy of several machine learning models for damage characterization, trained and tested on the database of damage observed after Italian earthquakes (DaDO). Six models were considered: regression- and classification-based machine learning models, each using random forest, gradient boosting and extreme gradient boosting. The structural features considered were divided into two groups: all structural features provided by DaDO or only those considered to be the most reliable and easiest to collect (age, number of storeys, floor area, building height). Macroseismic intensity was also included as an input feature. The seismic damage per building was determined according to the EMS-98 scale observed after seven significant earthquakes occurring in several Italian regions. The results showed that extreme gradient boosting classification is statistically the most efficient method, particularly when considering the basic structural features and grouping the damage according to the traffic-light based system used, for example, during the post-disaster period (green, yellow and red), 68% buildings were correctly classified. The results obtained by the machine learning-based heuristic model for damage assessment are of the same order of accuracy (error values were less than 17%) as those obtained by the traditional Risk-UE method. Finally, the machine learning analysis found that the importance of structural features with respect to damage was conditioned by the level of damage considered.

Key Words

Earthquake building-damage, DaDO building damage database, Machine learning, RISK-UE, Seismic vulnerability of buildings, Italy.

37 **1. Introduction**

38 Population growth worldwide increases exposure to natural hazards, increasing consequences in terms
39 of global economic and human losses. For example, between 1985 and 2014, the world's population
40 increased by 50% and average annual losses due to natural disasters increased from US\$14 billion to
41 over US\$140 billion (Silva et al., 2019). Among other natural hazards, earthquakes represent one-fifth
42 of total annual economic losses and cause more than 20 thousand deaths per year (Daniell et al., 2017;
43 Silva et al., 2019). To develop effective seismic risk reduction policies, decision-makers and
44 stakeholders rely on a representation of consequences when earthquakes affect the built environment.
45 Two main risk metrics generally considered at the global scale are associated with building damage:
46 direct economic losses due to costs of repair/replacement and loss of life of inhabitants due to building
47 damage. The damage is estimated by combining the seismic hazard, exposure models and
48 vulnerability/fragility functions (Silva et al., 2019).

49 For scenario-based risk assessment, damage and related consequences are computed for a single
50 earthquake defined in terms of magnitude, location, and other seismological features. Many methods
51 have been developed to characterize the urban environment for exposure models. In particular, damage
52 assessment requires vulnerability/fragility functions for all types of existing buildings, defined
53 according to their design characteristics (shape, position, materials, height, etc.) and grouped in a
54 building taxonomy (e.g. among other conventional methods FEMA, 2003; Grünthal, 1998; Guéguen
55 et al., 2007; Lagomarsino & Giovinazzi, 2006; Mouroux & Le Brun, 2006; Silva et al., 2014). At the
56 regional/country scale, damage assessment is therefore confronted with the difficulty of accurately
57 characterizing exposure according to the required criteria and assigning appropriate
58 vulnerability/fragility functions to building features. Unfortunately, the necessary information is often
59 sparse and incomplete, and exposure model is suffering from economic and time constraints.

60 Over the past decade, there has been growing interest in artificial intelligence methods for seismic risk
61 assessment, due to its superior computational efficiency, easy handling of complex problems, and the
62 incorporation of uncertainties (e.g., Riedel et al., 2014, 2015; Azimi et al., 2020; Ghimire et al., 2022;
63 Hegde and Rokseth, 2020; Kim et al., 2020; Mangalathu & Jeon, 2020; Morfidis & Kostinakis, 2018;
64 Salehi & Burgueño, 2018; Seo et al., 2012; Sun et al., 2021; Wang et al., 2021; Xie et al., 2020; Y. Xu
65 et al., 2020; Z. Xu et al., 2020). In particular, several studies have tested the effectiveness of machine
66 learning methods in associating damage degrees with basic building features and spatially-distributed
67 seismic demand with acceptable accuracy compared with conventional methods or tested with post-
68 earthquake observations (e.g., Riedel et al., 2014, 2015; Guettiche et al., 2017; Harirchian et al., 2021;
69 Mangalathu et al., 2020; Roeslin et al., 2020; Stojadinović et al., 2021; Ghimire et al., 2022). In parallel,
70 significant efforts have been made to collect post-earthquake building damage observations after
71 damaging earthquakes (Dolce et al., 2019; MINVU, 2010; MTPTC, 2010; NPC, 2015). With more than
72 10,000 samples compiled, the Database of Observed Damage (DaDO) in Italy, a platform of the Civil

73 Protection Department, developed by the Eucentre Foundation (Dolce et al., 2019), allows exploration
 74 of the value of heuristic vulnerability functions calibrated on observations (Lagomarsino et al., 2021),
 75 as well as the training of heuristic functions using machine learning models (Ghimire et al., 2022) and
 76 considering sparse and incomplete building features.

77 The main objective of this study is to investigate the effectiveness of several machine learning models
 78 trained and tested on information from the DaDO to develop a heuristic model for damage assessment.
 79 The model may be classified as heuristic because it applies a problem-solving approach in which a
 80 calculated guess based on previous experience is considered for damage assessment (as opposed to
 81 applying algorithms that effectively eliminate the approximation). The damage is thus estimated in a
 82 non-rigorous way defined during the training phase and the results must be validated and then tested
 83 against observed damage. By analogy with psychology, this procedure can reduce the cognitive load
 84 associated with uncertainties when making decisions based on damage assessment, by explicitly
 85 considering the uncertainties in the assessment, being aware about the incompleteness of the
 86 information and the accuracy level to make a decision. The dataset and methods are described in the
 87 data and method sections, respectively. The fourth section presents the results of damage prediction
 88 produced by machine learning models compared with conventional methods, followed by a conclusion
 89 section.

90

91 2. Data

92 The Database of Observed Damage (DaDO, Dolce et al., 2019) is accessible through a web-GIS
 93 platform and is designed to collect and share information about building features, seismic ground
 94 motions and observed damage following major earthquakes in Italy from 1976 to 2019. A framework
 95 was adopted to homogenize the different forms of information collected and to translate the damage
 96 information into the EMS-98 scale (Grunthal et al., 1998) using the method proposed by Dolce et al.
 97 (2019). For this study, we selected building damage data from seven earthquakes summarized in Table
 98 1 and presented in Fig.1.

99

100 **Table 1.** Building-damage data from the DaDO for the seven earthquakes considered in this study. ‘Ref’
 101 is the reference to the earthquake used in the manuscript. ‘DL’ is the number of the damage grade
 102 available in DaDO. ‘NB’ is the number of buildings considered in this study. AeDES is the post-
 103 earthquake damage survey form, first introduced in 1997 and become the official operational tool
 104 recognized by the Italian Civil Protection in 2002.

Ref	Earthquake	Event date	Mag.	Epicentre		Damage survey form	DL	NB
				Lat.	Long.			
E1	Irpinia-1980	23/11/1980	6.9	40.91	15.37	Irpinia-980	8	37,828
E2	Pollino-1998	09/09/1998	5.6	40.04	15.98	AeDES-1998	4	9,485
E3	Molise-Puglia-2002	31/10/2002	5.9	41.79	14.87	AeDES-2000	4	6,396

E4	Emilia-Romagna-2003	14/09/2003	5.3	44.33	11.45	AeDES-2000	4	239
E5	L'Aquila-2009	06/04/2009	6.3	42.34	13.34	AeDES-2008	4	37,999
E6	Emilia-Romagna-2012	20/05/2012	6.1	44.89	11.23	AeDES-2008	4	10,581
E7	Garfagnana-Lunigiana-2013	21/06/2013	5.3	44.15	10.14	AeDES-2008	4	1,474

105

106 The converted EMS-98 damage grade (DG) ranges from damage grade DG0 (no damage) to DG5 (total
107 collapse). The building features are available for each individual building and relate to the shape and
108 design of the building and the built-up environment (Tab. 2, Fig. 2), as follows:

109 **Building location** - the location of each building is defined by its latitude and longitude, assigned using
110 either the exact address of the building if available or the address of the local administrative centre
111 (Dolce et al., 2019).

112 **Numbers of storeys** - total number of floors above the surface of the ground.

113 **Age of building** - time difference between the date of the earthquake and the date of building
114 construction/renovation.

115 **Height of building** - total height of the building above the surface of the ground, in m.

116 **Floor area** – average of the storey surface area, in m².

117 **Ground slope condition** - four types of ground slope conditions are defined (flat, mild slope, steep
118 slope, and ridge).

119 **Roof type** – four types of roofs are defined (thrusting heavy roof, non-thrusting heavy roof, thrusting
120 light roof, and non-thrusting light roof).

121 **Position of building** - indication of the building's position in the block: isolated, extreme, corner, and
122 intermediate.

123 **Regularity**: building regularity in terms of plan and elevation, classified as either irregular or regular.

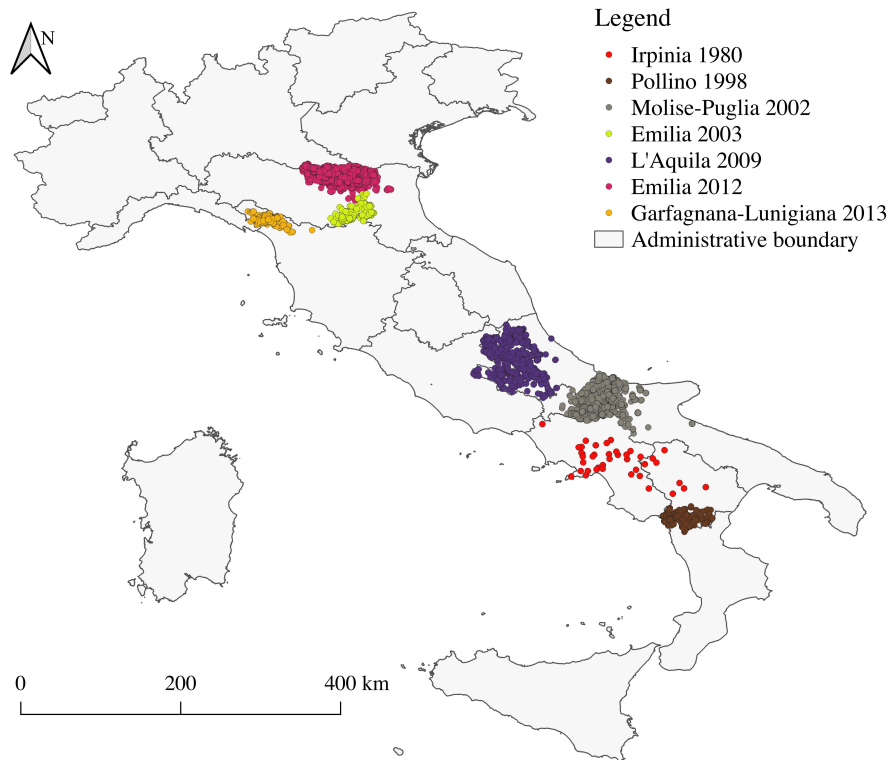
124 **Construction material**: vertical elements: good and poor-quality masonry, good and poor quality
125 mixed frame masonry, reinforced concrete frame and wall, steel frame, and other.

126 For features defined as value ranges (e.g., date of construction/renovation, floor area, and building
127 height), the average value was used. Furthermore, the Irpinia-1980 building damage portfolio (E1) was
128 constructed using the specific Irpinia-1980 damage survey form, while the AeDES damage survey form
129 was used for the others. The Irpinia-1980 dataset will therefore be analysed separately.

130 Building damage data from earthquake surveys other than the Irpinia-1980 earthquake damage survey
131 primarily include damaged buildings. This is because the data was collected based on requests for
132 damage assessments after the earthquake event (Dolce et al. 2019). The damage information in the
133 DaDO database is still relevant for testing the machine learning models for heuristic damage
134 assessment. Mixing these datasets to train machine learning models can lead to biased outcomes.
135 Therefore, the machine learning models were developed on the other earthquake dataset excluding the
136 Irpinia dataset, and the Irpinia earthquake dataset was used only in the testing phase.

137 The distribution of the samples is very imbalanced (Fig. 2): for example, there is a small proportion of
138 buildings in DG4+DG5 (7.59%), and a large majority of masonry (65.47%) compared to reinforced

139 concrete frame (21.31%) buildings. This imbalance should be taken into account when defining the
 140 machine learning models.
 141



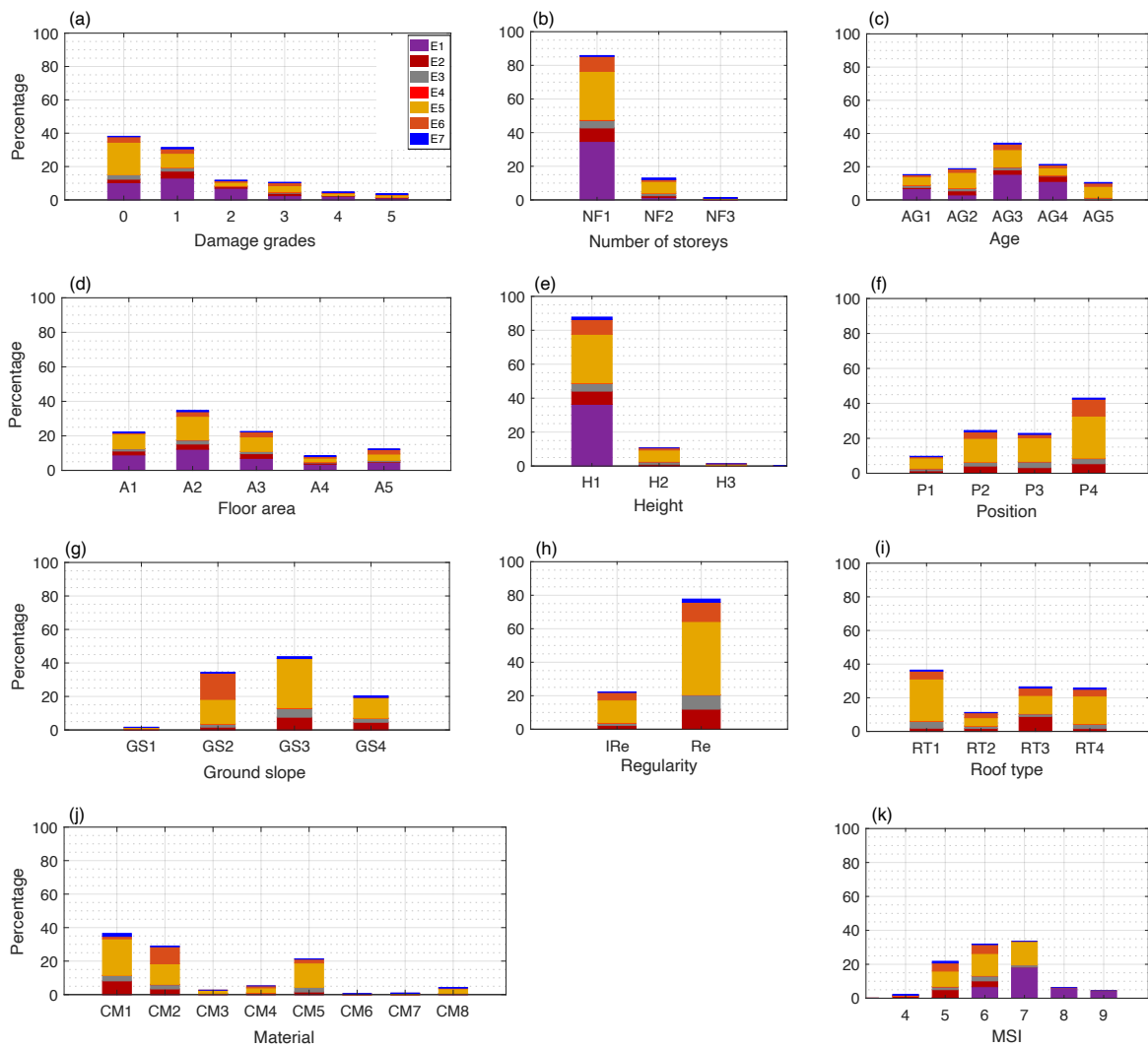
142
 143 **Figure 1.** Geographic location of the buildings considered in this study.
 144

145 To consider spatially-distributed ground motion, the original DaDO data are supplemented with the
 146 main event macroseismic intensities (MSI) provided by the United States Geological Survey (USGS)
 147 ShakeMap tool (Wald et al., 2005). Macroseismic intensities (MSI) given in terms of modified Mercalli
 148 intensities are considered and assigned to buildings based on their location. The distribution of MSI
 149 values in the database is shown in Fig. 2k.

150
 151 **Table 2.** Distribution of the different features used in this study.

No.	Parameters	Data type	Distribution (%)	Remarks
1	No damage	DG0	43.63	Fig. 2a
	Slight damage	DG1	28.90	
	Moderate damage	DG2	7.41	
	Substantial damage	DG3	12.48	
	Very heavy damage	DG4	3.94	
	Total collapse	DG5	3.65	
2	0-3	NF1	85.81	Fig. 2b
	3-5	NF2	13.01	
	> 5	NF3	1.19	

3	Age (years)	0-20	AG1	Numerical	15.22	Fig. 2c
		21-40	AG2		18.81	
		41-60	AG3		34.15	
		61-80	AG4		21.34	
		>80	AG5		10.49	
4	Floor area (square metres)	0-50	A1	Numerical	22.16	Fig. 2d
		50-100	A2		34.73	
		100-150	A3		22.53	
		150-200	A4		8.32	
		> 200	A5		12.26	
5	Height (metres)	0-10	H1	Numerical	87.78	Fig. 2e
		10-15	H2		10.69	
		>15	H3		1.50	
6	Position	Corner	P1	Categorical	9.71	Fig. 2f
		Extreme	P2		24.47	
		Internal	P3		22.80	
		Isolated	P4		43.02	
7	Ground slope	Ridge	GS1	Categorical	2.62	Fig. 2g
		Plain	GS2		34.25	
		Moderate slope	GS3		43.74	
		Steep Slope	GS4		20.39	
8	Regularit y	Irregular in plan and elevation	IR	Categorical	22.28	Fig. 2h
		Regular in plan and elevation	Re		77.72	
9	Roof type	Heavy no thrust	R1	Categorical	36.43	Fig. 2i
		Heavy thrust	R2		11.25	
		Light thrust	R3		26.48	
		Light no thrust	R4		25.83	
10	Material	Masonry poor quality	CM1	Categorical	36.51	Fig. 2j
		Masonry good quality	CM2		28.96	
		Mixed frame masonry poor quality	CM3		2.64	
		Mixed frame masonry good quality	CM4		5.21	
		Reinforced concrete frame	CM5		21.31	
		Reinforced concrete wall	CM6		0.42	
		Steel frame	CM7		0.09	
		Other	CM8		4.10	



153

154 **Figure 2.** Distribution of the different features in the database. E1, E2, E3, E4, E5, E6, and E7, representing
 155 Irpinia-1980, Pollino-1998, Molise-Puglia-2002, Emilia-Romagna-2003, L'Aquila-2009, Emilia-Romagna-2012,
 156 and Garfagnana-Lunigiana-2013 building damage portfolios, respectively. The y-axis is the percentage
 157 distribution and the x-axis is (a) Damage grade, (b) Number of storeys (NF1: 0-3, NF2: 3-5, NF3: >5), (c) Building
 158 age (AG1: 0-20, AG2: 21-40, AG3: 41-60, AG4: 61-80, AG5: >80), (d) Floor area (A1: 0-50, A2: 51-100, A3:
 159 101-150, A4: 151-200, A5: >200), (e) Height (H1: 0-10, H2: 10-15, H3: >15), (f) Building position (P1: corner,
 160 P2: extreme, P3: internal, P4: isolated), (g) Ground slope condition (GS1: ridge, GS2: plain, GS3: moderate slope,
 161 GS4: steep slope), (h) Regularity in plan and elevation (IRe: irregular, Re: Regular), (i) Roof type (RT1: heavy
 162 no thrust, RT2: heavy thrust, RT3: light no thrust, RT4: light thrust), (j) Construction material (CM1: poor-quality
 163 masonry, CM2: good-quality masonry, CM3: poor-quality mixed frame masonry, CM4: good-quality mixed
 164 frame masonry, CM5: reinforced concrete frame, CM6: reinforced concrete wall, CM7: steel frames, CM8: other),
 165 and (k) macro-seismic intensity.

166

167 **3. Method**

168 **3.1. Machine learning models**

169 Ghimire et al. (2022) applied classification- and regression-based machine learning models to the
170 damage observed after the 2015 Gorkha Nepal earthquake (NPC, 2015). The main concepts for method
171 selection, the definition of the dataset for training and testing, and the representation of model
172 performance are presented here.

173 To develop the heuristic damage assessment model, the damage grades are considered as the target
174 feature. The damage grades are discrete labels, from DG0 to DG5. Three most advanced classification
175 and regression machine learning algorithms were selected: random forest (RFC) and regression (RFR)
176 (Breiman, 2001), gradient boosting classification (GBC) and regression (GBR) (Friedman, 1999), and
177 extreme gradient boosting classification (XGBC) and regression (XGBR) (Chen and Guestrin, 2016).
178 A label (or class) was thus assigned to the categorical response variables (DG) for the classification-
179 based machine learning models. For the regression-based machine learning models, DG is converted
180 into a continuous variable to minimize misclassifications (Ghimire et al., 2022).

181 Building features and macroseismic intensities were considered as input features. A one-hot encoding
182 technique was used to convert the categorical features (i.e., ground slope condition, building position,
183 roof type, construction material) into binary values (1 or 0), resulting in 28 input variables (Tab. 2). No
184 input features were removed from the dataset: some building features (e.g., number of storeys and
185 height) may be correlated but we assumed that the presence of correlated features does not impact the
186 overall performance of these machine learning methods (Ghimire et al., 2022). No specific data cleaning
187 methods were applied to the DaDO database.

188 The machine learning algorithms from the Scikit-learn package developed in Python (Pedregosa et al.,
189 2011) were applied. The machine learning models were trained and tested on the randomly selected
190 training (60% of the dataset) and testing (40% of the dataset) subsets of data, considering a single
191 earthquake dataset or the whole DaDO dataset. The testing subset was kept hidden from the model
192 during the training phase.

193

194 **3.2. Machine learning model efficacy**

195 The efficacy of the heuristic damage assessment model (i.e., its ability to predict damage to a
196 satisfactory or expected degree) was analysed in three stages: comparison of the efficacy of the machine
197 learning models using metrics; analysis of specific issues related to machine learning using the selected
198 models; and application of the heuristic model to the whole DaDO dataset.

199

200 **3.2.1 First stage: model selection**

201 In the first stage, only the L'Aquila-2009 portfolio was considered for the training and testing phases.
202 This is the largest dataset in terms of the number of buildings and was obtained using the AeDES survey
203 format (Baggio et al., 2007; Dolce et al., 2019). Model efficacy was provided by the confusion matrix,

204 which represents model prediction compared with the so-called “ground truth” value. Accuracy was
205 then represented on the confusion matrix by the ratio of the number of correctly predicted DGs to the
206 total number of observed values per DG (A_{DG}).

207 Total accuracy (A_T) was computed as the ratio of the number of correctly predicted DGs to the total
208 number of observed values. A_T and A_{DG} values close to 1 indicate high efficacy. Moreover, the
209 quantitative statistical error was also calculated as the mean of the absolute value of errors (MAE) and
210 the mean squared error (MSE) (MAE and MSE values close to 0 indicate high efficacy). For
211 classification-based machine learning models, the ordinal value of the DG was used to calculate the
212 MAE and MSE scores directly. For the regression-based machine learning models, the output DG
213 values were rounded to the nearest integer for the accuracy scores plotted for the confusion matrix, but
214 not for the MAE and MSE value calculations.

215

216 **3.2.2 Second stage: machine learning related issues**

217 In the second stage, the best heuristic model for damage assessment was selected based on the highest
218 efficacy, and used to analyse and test specific issues related to machine learning: (1) the imbalance
219 distribution of DGs in the DaDO, (2) the performance of the selected model when only some basic, but
220 accurately assessed, building features are considered (i.e., number of storeys, location, age, floor area),
221 and (3) the simplification of the heuristic model, in the sense that DGs are grouped into a traffic-light-
222 based classification (i.e., green, yellow and red, corresponding to DG0+DG1, DG2+DG3 and
223 DG4+DG5, respectively). In the second stage, the issues related to machine learning were first analysed
224 using the L’Aquila-2009 portfolio. The whole DaDO dataset was then used.

225

226 **3.2.2 Third stage: application to the whole DaDO portfolio and comparison with Risk-UE**

227 In the third stage, several learning and testing sequences were considered, with the idea of moving to
228 an operational configuration in which past information is used to predict damage from future
229 earthquakes: either learning based on a portfolio of damage caused by one earthquake and tested on
230 another portfolio, or learning based on a series of damage portfolios and tested on the portfolio of
231 damage caused by an earthquake placed in the chronological continuity of the earthquake sequence
232 considered. In this stage, the efficacy of the heuristic damage assessment model was analysed by
233 comparing the prediction values with the so-called “ground truth” values through the error distribution,
234 as follows:

$$235 \quad \varepsilon_d(\%) = \left(\frac{n_e}{N}\right) * 100 \quad (1)$$

236 where n_e is the total number of buildings at a given error level (difference between observed and
237 predicted DGs), N is the total number of buildings in the damage portfolio.

238 In this stage, the efficacy of the heuristic damage assessment model was compared with the
239 conventional damage prediction framework proposed by the RISK-UE method (Milutinovic and

240 Trendafiloski, 2003). The RISK-UE method assigns a vulnerability index (IV) to a building, based on
 241 its construction material and structural properties (e.g., height, building age, position, regularities,
 242 geographic location, etc.). For a given level of seismic demand (MSI), the mean damage (μ_d) and the
 243 probability, p_k , of observing a given damage level k ($k = 0$ to 5) are given by:

244

$$245 \mu_d = 2.5 \left[1 + \tanh \left(\frac{MSI + 6.25IV - 13.1}{2.3} \right) \right] \quad (2)$$

246

$$247 p_k = \frac{5!}{k!(5-k)!} \left(\frac{\mu_d}{5} \right)^k \left(1 - \frac{\mu_d}{5} \right)^{5-k} \quad (3)$$

248

249 Herein, comparing the heuristic model and the RISK-UE method amounts to considering the following
 250 steps, based on the equations given by RISK-UE:

251 **Step 1** - The buildings in the training and testing datasets are grouped into different classes according
 252 to construction material.

253 **Step 2** - For a given building class in the training dataset, computation of

254 **Step 2.1** - mean damage (μ_d) using the observed damage distribution at a given MSI value by:

$$255 \mu_d = \sum_{k=0}^5 p_k k \quad (4)$$

256

257 **Step 2.2** - vulnerability index (IV) with the μ_d obtained in step 2.1 by:

258

$$259 IV = \frac{1}{6.25} \left[13.1 - MSI + 2.3 \left(\tanh^{-1} \left(\frac{\mu_d}{2.5} - 1 \right) \right) \right] \quad (5)$$

260

261 **Step 3** - For the same building class in the test dataset, calculation of

262 **Step 3.1** - mean damage (μ_d) Eq. 2 for a given MSI value with the value of IV obtained in step
 263 2.2;

264 **Step 3.2** - damage probability (p_k) Eq. 3 with the value of μ_d obtained in step 3.1;

265 **Step 3.3** - distribution of buildings in each damage grade within a range of MSI values observed
 266 in the test dataset as follows:

267

$$268 N_{pred,k} = \sum_{MSI} p_k n_{obs,MSI} \quad (6)$$

269

270 where $n_{obs,MSI}$ is the total number of buildings observed in the test set for a given MSI
 271 value;

272 **Step 3.4** - absolute error (ε_k) in each damage level k , given by:

$$273 \varepsilon_k = \left| \frac{N_{obs,k} - N_{pred,k}}{N} \right| \quad (7)$$

274

275

where, $N_{obs,k}$ is the total number of buildings observed in the given damage grade k .

276

277

Similarly, the heuristic damage assessment model was also compared with the mean damage

278

relationship (Eq. 4) applied to the test set. Thus, for each building class in the test set, the error value

279

(Eq. 7) for each DG was computed from the μ_d on the observed damage using Eq. (4), the probability

280

p_k of obtaining a given DG k ($k= 0$ to 5) using Eq. (3), and the distribution of buildings in each DG

281

$N_{pred,k}$ for a given MSI value using Eq. (6).

282

283 4. Result

284 4.1 First stage: model selection

285

The efficacy of the regression (RFR, GBR, XGBR) and classification (RFC, GBC, XGBC) machine

286

learning models trained and tested on the randomly selected 60% (training set) and 40% (test set) of the

287

2009 -L'Aquila earthquake building damage portfolio is summarized in Table 3. The hyperparameters

288

indicated in Tab. 3 were chosen after tests performed by Ghimire et al. (2021). The regression-based

289

machine learning models RFR, GBR and XGBR yielded similar MSE scores (1.22, 1.22 and 1.21) and

290

accuracy scores ($A_T = 0.49, 0.50$ and 0.50), considering the five DGs of the EMS-98 scale. In the

291

confusion matrix (Fig. 3a: RFR, Fig. 3b: GBR, and Fig. 3c: XGBR), the accuracy A_{DG} values show that

292

the efficacy of these models is higher for the lower DGs (around 60% for DG0 and 55% for DG1) and

293

lower for the higher DGs (6% and 1% of the buildings are correctly classified in DG4 and DG5,

294

respectively).

295

For the classification-based machine learning models, the XGBC model ($[MSE, A_T] = [1.78, 0.59]$) was

296

more effective than the RFC ($[MSE, A_T] = [1.86, 0.57]$) and GBC ($[MSE, A_T] = [1.80, 0.58]$) models,

297

considering the EMS-98 scale. In the confusion matrix (Fig. 3d: RFC, Fig. 3e: GBC, and Fig. 3f:

298

XGBC), the accuracy A_{DG} values also show higher model efficacy for the lower DGs (86% for DG0

299

and 39% for DG1) and lower efficacy for the higher DGs (5%, 23%, 12% and 17% buildings correctly

300

classified in DG2, DG3, DG4 and DG5, respectively).

301

302 **Table 3.** Summary of optimized hyperparameters parameters, accuracy A_T and quantitative statistical

303

error values for the regression-based and classification-based machine learning methods. The

304

parameters are the hyperparameters chosen for the machine learning models (the other hyperparameters

305

not mentioned here are the default parameters in the Scikit-learn documentation (Pedregosa et al.,

306

2011)). The best accuracy and error values are indicated in bold.

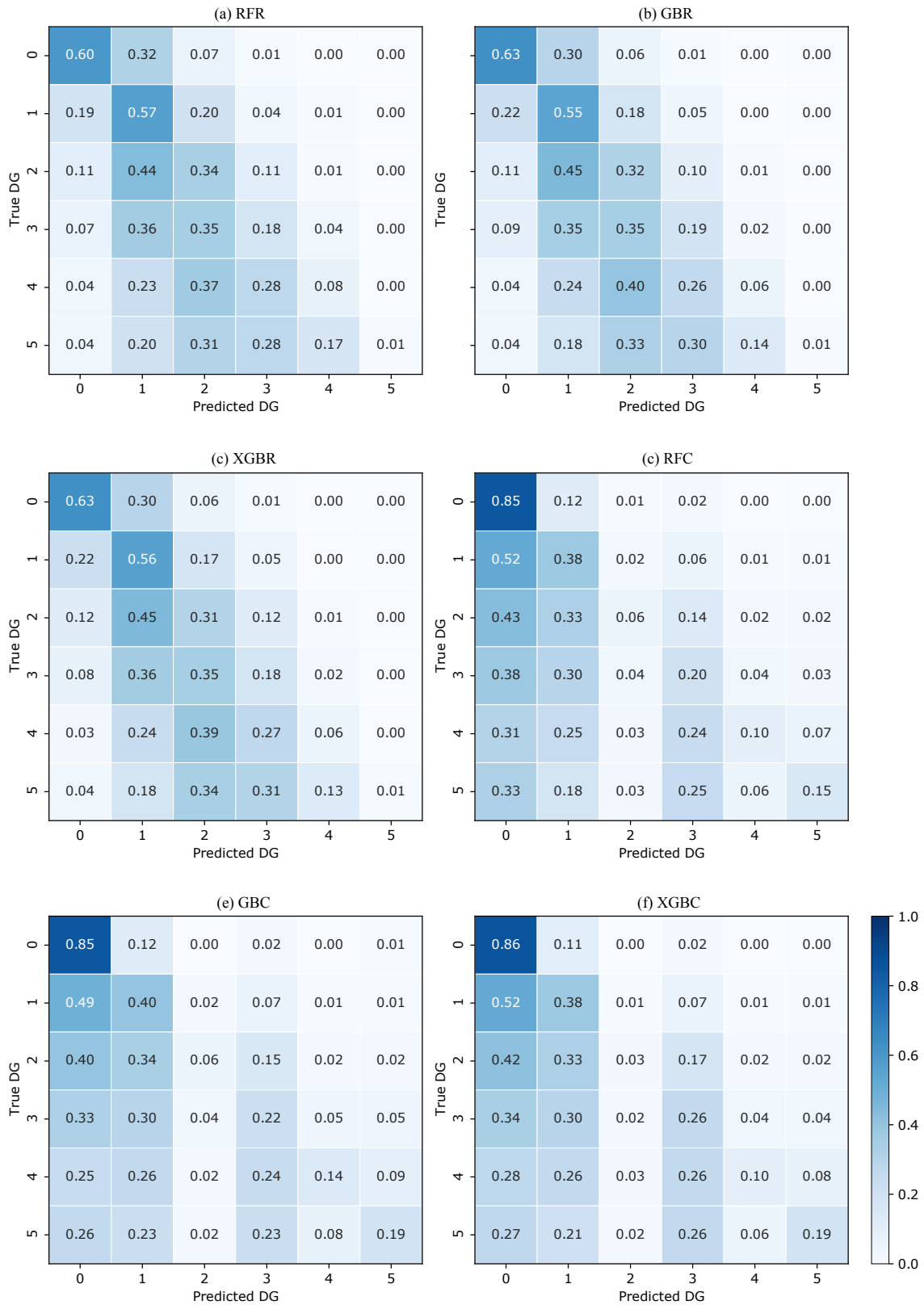
Method	Parameters	Accuracy A_T	MSE	MAE
RFR	n_estimators = 1000	0.49	1.22	0.77

	max_depth = 25			
GBR	n_estimators = 1000 max_depth = 10 learning_rate = 0.01	0.50	1.22	0.77
XGBR	n_estimators = 1000 max_depth = 10 learning_rate = 0.01	0.50	1.21	0.76
RFC	no_estimators = 1000 max_depth = 25	0.57	1.86	0.77
GBC	no_estimators = 1000 max_depth = 10 learning_rate = 0.01	0.58	1.80	0.77
XGBC	n_estimators = 1000 max_depth = 10 learning_rate = 0.01	0.59	1.78	0.74

307

308 The classification-based machine learning models thus yielded slightly better predictive efficacy, but
309 still lower than recent studies applied to other datasets (Ghimire et al., 2022; Harirchian et al., 2021;
310 Mangalathu et al., 2020; Roeslin et al., 2020; Stojadinović et al., 2021). The high classification error in
311 the higher DGs could be related to the characteristics of the building portfolio and the imbalance of DG
312 distribution. Among the classification methods, the XGBC model showed slightly higher classification
313 efficacy; the XGBC model was therefore selected for the next stages 2 and 3.

314



315

316 **Figure 3.** Normalized confusion matrix between predicted and observed DGs. The values given in each main
 317 diagonal cell are the accuracy scores A_{DG} . All values are also represented by the colour scale.

318

319 **4.2 Second stage: issues related to machine learning**

320 **4.2.1 Imbalance distribution of the DGs in the DaDO**

321 The efficacy of the heuristic damage assessment model depends on the distribution of target features in
 322 the training dataset. This can lead to low prediction efficacy, especially for minority classes (Estabrooks
 323 & Japkowicz 2001; Japkowicz & Stephen 2002; Branco et al. 2017; Ghimire et al., 2022). The previous
 324 section reports significant misclassification associated with the highest DGs for all classification- and
 325 regression-based models (Fig. 3), i.e., for the DGs with the lowest number of buildings (Fig. 2a). The
 326 efficacy of the XGBC model is analysed below, addressing the class-imbalance issue with data
 327 resampling techniques applied to the training phase and considering the L’Aquila-2009 portfolio.

328

329 Four strategies to solve the class imbalance issue were tested:

330 (a) random undersampling: randomly selecting the number of data entries in each class equal to the
 331 number of data entries in the minority class (DG4 in our case);

332 (b) random oversampling: randomly replacing the number of data entries in each class equal to the
 333 number of data entries in the majority class (DG0 in our case);

334 (c) Synthetic Minority Oversampling Technique (SMOTE): creating an equal number of data entries in
 335 each class by generating synthetic samples by interpolating the neighbouring data in the minority class;

336 (d) a combination of oversampling and undersampling methods: oversampling of the minority class
 337 using the SMOTE method, followed by the Edited Nearest Neighbours (ENN) undersampling method
 338 to eliminate data that is misclassified by its three nearest neighbours (SMOTE-ENN).

339

340 Fig. 4 shows the confusion matrices of the four strategies considered for the class imbalance issue.
 341 Compared with Fig. 3f (i.e., XGBC), the effects of addressing the issue of imbalance were as follows:

342 (a) undersampling (Fig. 4a): A_{DG} value increased by 20/22/26% for DG2/DG4/DG5 and decreased by
 343 29% for DG0.

344 (b) oversampling (Fig. 4b): A_{DG} value increased by 11/16/18% for DG2/DG4/DG5 and decreased by
 345 13% for DG0

346 (c) SMOTE (Fig. 4c): A_{DG} value increased by 4/1/4% for DG2/DG4/DG5 and decreased by 3% for
 347 DG0

348 (d) SMOTE-ENN (Fig. 4d): A_{DG} value increased by 13/9/8% for DG2/DG4/DG5 and decreased by 25%
 349 for DG0.

350 The A_T , MAE and MSE scores are given in Table 4 with the associated effects.

351

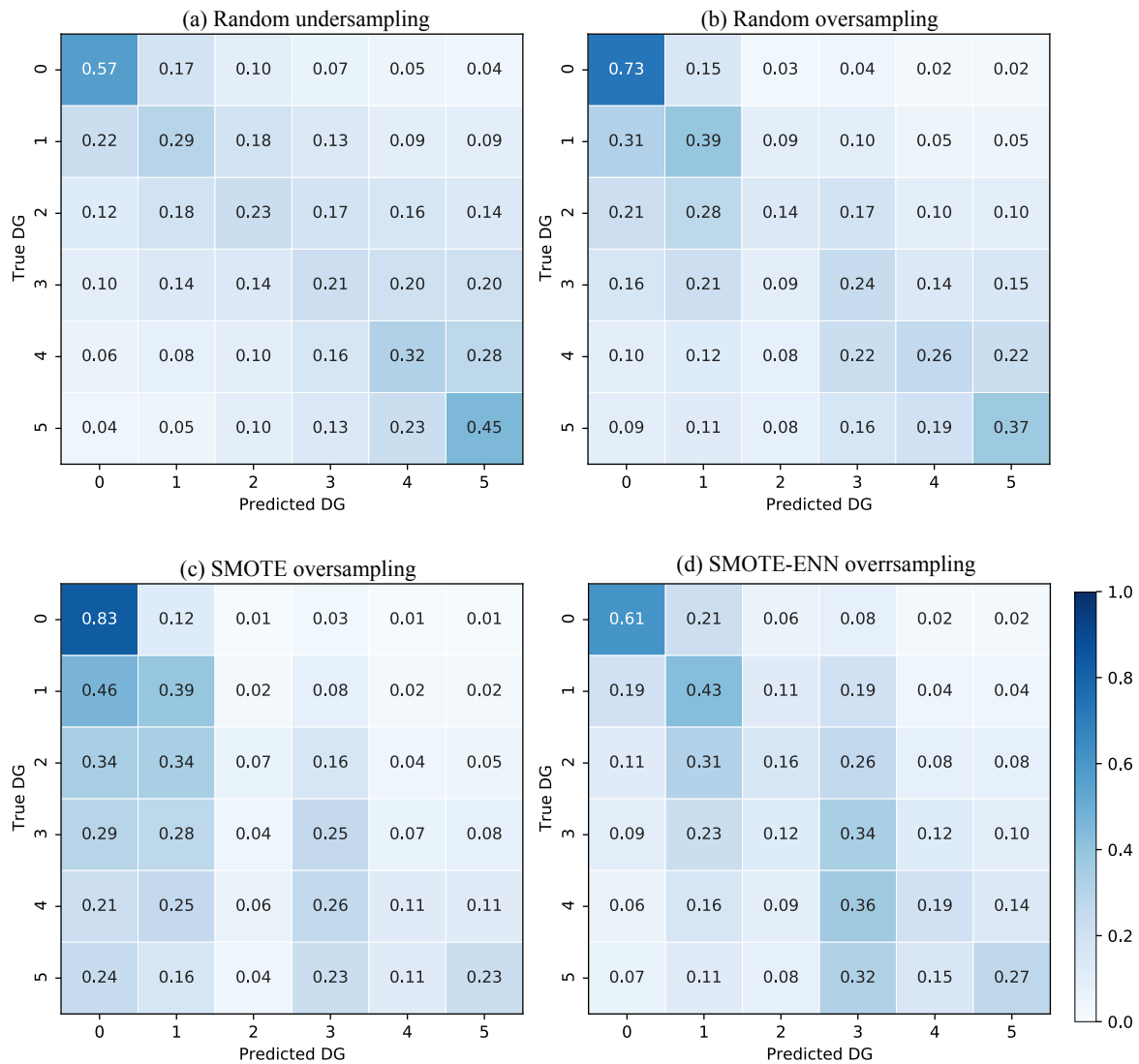
352 Table 4 – Scores of the accuracy A_T , MSE and MAE metrics considering the imbalance issue and their
 353 variation Δ compared with values without consideration of the imbalance.

Method	Accuracy A_T		MSE		MAE	
	Scores	Δ	Score	Δ	Score	Δ

Undersampling	0.26	-0.33	1.24	-0.34	1.20	0.46
Oversampling	0.53	-0.06	2.13	0.35	0.86	0.12
SMOTE	0.57	-0.02	1.87	0.09	0.77	0.03
SMOTE-ENN	0.49	-0.10	2.28	0.50	0.93	0.19

354

355 In conclusion, the random oversampling method improves prediction in the minority class without
 356 significantly decreasing prediction in the majority class. The random oversampling method was
 357 therefore applied in this study.



358

359 **Figure 4.** Confusion matrices for the four methods to solve the DG imbalance issue in the DaDO. The values
 360 given in each main diagonal cell are the accuracy scores A_{DG} . All values are also represented by the colour scale.

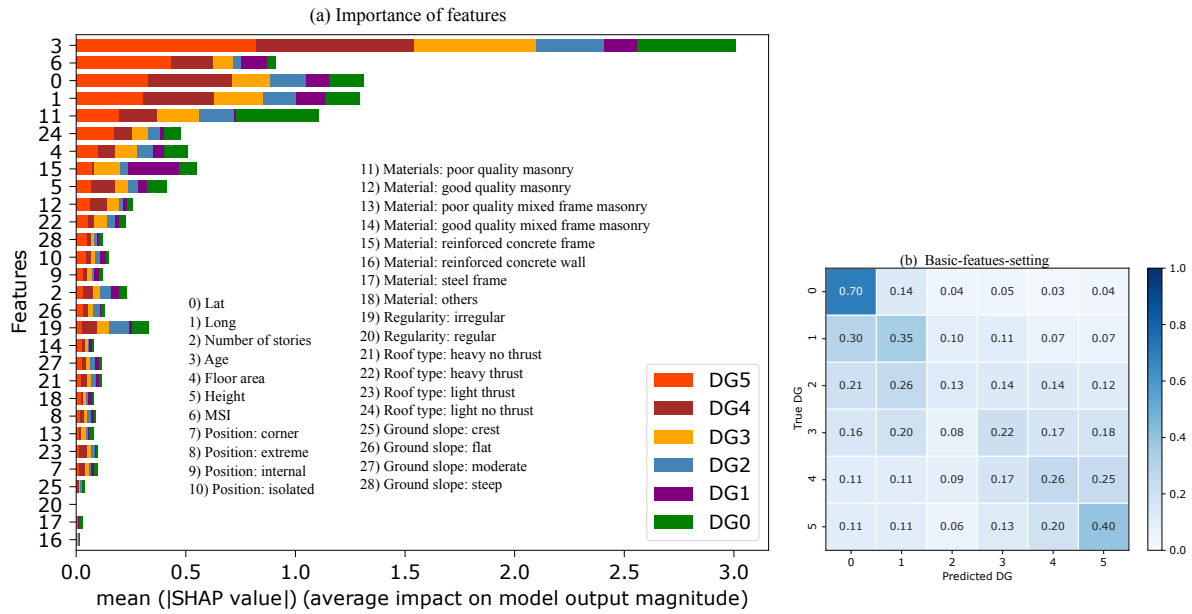
361

362 **4.2.2 Testing the XBGC model with basic features**

363 This section begins by exploring the importance of each feature in the heuristic damage assessment
364 model applied to the L'Aquila-2009 portfolio. We used the Shapely Additive Explanations (SHAP)
365 method developed by Lundberg and Lee (2017). The SHAP method compares the efficacy of the model
366 with and without considering each input feature to measure its average impact, provided in terms of
367 mean absolute SHAP values.

368 Figure 5a shows the average SHAP value associated with each feature considered in this study as a
369 function of DG. The most weighted features are building age, location (latitude and longitude), material
370 (poor quality masonry, RC frame), MSI, roof type, floor area, and height. Interestingly, the mean SHAP
371 values are dependent on the DG, i.e., the weight of the feature is not linear depending on the DG
372 considered; this is never taken into account in vulnerability methods. For example, Scala et al. (2022)
373 and Del Gaudio et al. (2021) observed a decrease in the vulnerability of structures as construction year
374 increases, without distinguishing the DG considered, which is not the case herein. Note also that the
375 importance score associated with the location feature can indirectly capture variations in local
376 geological properties and the spatially distributed vulnerability associated with the built-up area of the
377 L'Aquila-2009 portfolio (e.g., the distinction between the historic town and more modern urban areas).
378 Furthermore, the average SHAP value obtained for poor quality masonry buildings for DG3/DG4/DG5
379 confirms the same high vulnerability of this typology as in the EMS-98 scale (Grünthal, 1998),
380 regardless of DG.

381 Some basic features of the building (e.g., location, age, floor area, number of storeys, height) are
382 observed with a high mean SHAP value (Fig. 5a). Compared with others, these five basic features can
383 be easily collected from the field or provided by national census databases, for example. Fig. 5b shows
384 the efficacy of the heuristic damage assessment model using XGBC trained with a set of easily
385 accessible building features (i.e., basic-features-setting: geographic location, floor area, number of
386 stories, height, age, MSI), after addressing the class-imbalance issue using the random oversampling
387 method. Compared with Fig. 4b (considering all features and named as the full-features-setting), the
388 XGBC model with the basic-features-setting (Fig. 5b) gives almost the same efficacy with only a 6%
389 average reduction in the accuracy scores.



390

391 **Figure 5.** (a) Graphic representation of the importance scores associated with the different input features
 392 considered for the XGBC model. The features (the same as in Fig. 2) considered in this study are on the y-axis,
 393 and the x-axis is the mean SHAP score according to DG. (b) Confusion matrices considering the basic-features-
 394 setting. The values given in each main diagonal cell are the accuracy scores A_{DG} . All values are also represented
 395 by the colour scale.

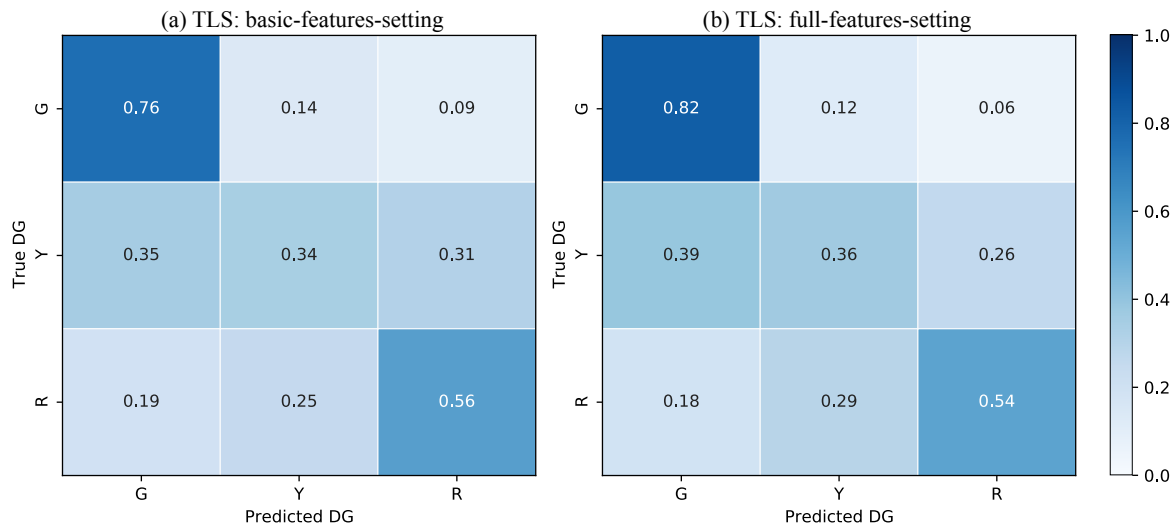
396

397 4.2.3 Testing the XGBC model with the traffic-light system for damage grades

398 In this section, a simplified version of the DG scale was used, in the sense that the DGs are classified
 399 according to a traffic-light system (TLS) (i.e., green G, yellow Y and red R classes, corresponding to
 400 DG0+DG1, DG2+DG3 and DG4+DG5, respectively), as monitored during post-earthquake emergency
 401 situations (Mangalathu et al., 2020; Riedel et al., 2015; ATC, 2005; Bazzurro et al., 2004). For the
 402 TLS-based damage classification, the XGBC model (after oversampling to compensate of the
 403 imbalance issue) with the basic-features-setting applied to the L'Aquila-2009 portfolio (Fig. 6a) gives
 404 almost the same efficacy compared to the full-features-setting (Fig. 6b). For example, accuracy values
 405 A_{DG} using the basic-features-setting and the full-features-setting were 0.76/0.34/0.56 and 0.82/0.36/0.54
 406 for G/Y/R classes, with the accuracy score A_T of 0.68 and 0.72, respectively. Mangalathu et al. (2020),
 407 Roslin et al., (2020), and Harirchian et al., (2021) reported similar damage grade classification accuracy
 408 values of 0.66, 0.67, and 0.65 respectively.

409 The efficacy of the heuristic damage assessment model using TLS-based damage classification
 410 indicates that classifying damage into three classes is much easier for the machine learning model
 411 compared with the six-class classification system (EMS-98 damage classification). This is also
 412 observed during damage surveys in the field, which sometimes find it hard to distinguish the
 413 intermediate damage grades, such as DG2 and DG3, or DG3 and DG4. Similar observations have been

414 reported in previous studies by Guettiche et al., (2017); Harirchian et al., (2021); Riedel et al., (2015);
 415 Roeslin et al., (2020) and Stojadinović et al., (2021).
 416



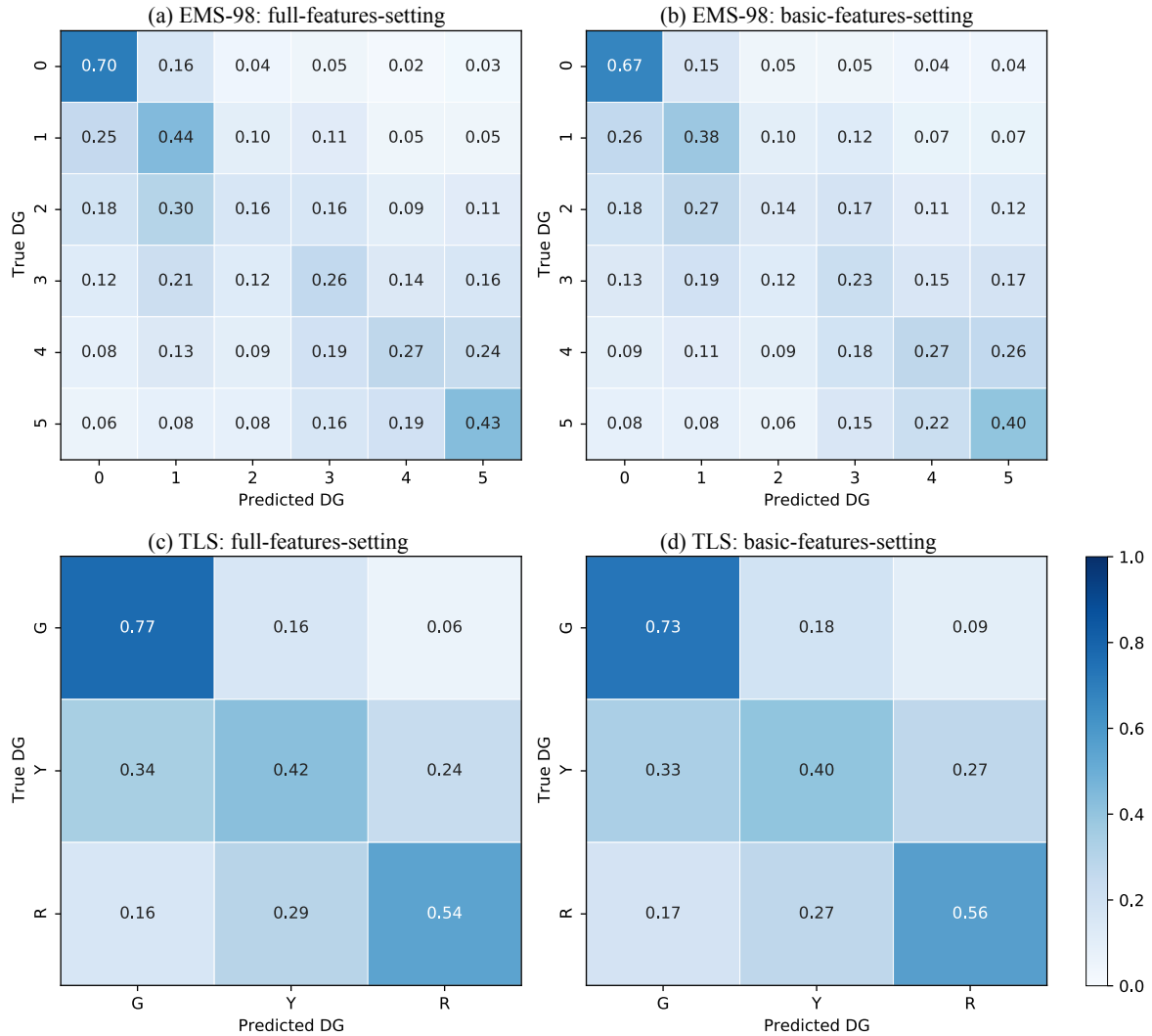
417
 418 **Figure 6.** Confusion matrices for (a) the basic-features-setting and (b) the full-features-setting using the traffic-
 419 light (TLS)-based classification, grouping the EMS-98 damage grades (DG) into three classes (green for no or
 420 slight damage; yellow for moderate damage; and red for heavy damage). The values given in each main diagonal
 421 cell are the accuracy scores A_{DG} . All values are also represented by the colour scale.
 422

423 4.2.4 Testing the XGBC model with the whole dataset

424 The efficacy of the XGBC model was tested using a dataset with six building damage portfolios,
 425 excluding the 1980-Irpinia building damage portfolio. The XGBC model was trained and tested on the
 426 randomly selected 60% (training set) and 40% (test set) of the dataset for EMS-98/TLS damage
 427 classification, with two sets of features (full-features-setting and basic-features-setting), applying the
 428 random oversampling method to compensate for class-imbalance issues. Fig.7 shows the associated
 429 confusion matrix.

430 The basic-features-setting resulted in a similar level of damage prediction compared with the full-
 431 features setting for both EMS-98 and TLS-based damage classification systems. For EMS-98 damage
 432 classification (Fig. 7a, b), the accuracy A_{DG} scores indicated in the confusion matrices are almost the
 433 same for the basic-features-setting and the full-features-setting. Furthermore, the accuracy A_T and MAE
 434 scores are also almost the same (0.45 and 1.08 for the basic-features-setting and 0.48 and 0.95 for the
 435 full-features-setting).

436 Likewise, for TLS-based damage classification (Fig. 7c, d), the accuracy values A_{DG} for the basic-
 437 features-setting and the full-features-setting are almost the same, with similar accuracy A_T and MAE
 438 scores (0.63/0.45 and 0.67/0.39, respectively).
 439
 440



441

442 **Figure 7.** Confusion matrices for EMS-98 (a, b) and TLS (c, d) damage classification systems using the basic-
 443 and full-features-settings (green for no or slight damage; yellow for moderate damage; red for heavy damage)
 444 with (c) the full-features-setting and (d) the basic-features-setting. The values given in each main diagonal cell
 445 are the accuracy scores A_{DG} . All values are also represented by the colour scale.

446

447 4.3 Third stage: application to the whole DaDO portfolio and comparison with Risk-UE

448 In this section, the efficacy of the heuristic damage assessment model was considered for building
 449 damage predictions, without respecting the time frame of the earthquakes. Two scenarios were
 450 considered: (1) a single building damage portfolio was used for training and the model was then tested
 451 on the others (named single-single), in situations using a single portfolio to predict future damage; and
 452 (2) some building damage portfolios were used for training but testing was performed on a single
 453 portfolio (named aggregate-single), i.e. a larger number of damage portfolios were used as a training
 454 set to predict the damage caused by the next earthquake. The model XGBC was applied with the basic-
 455 features-setting (number of storeys, building age, floor area, height, MSI for EMS-98) and EMS-98-
 456 and TLS-based damage classification.

457

458 **4.3.1 Single-single scenario**

459 First, a series of building damage portfolios, concerning earthquakes occurring in northern or southern
460 Italy and of different magnitudes, was used for training and testing:

461 (i) Training set: E3 – test set: E1, E5, E7.

462 (ii) Training set: E5 – test set: E1, E3, E7.

463 (iii) Training set: E7 – test set: E1, E3, E5.

464

465 Figure 8 shows the distribution of correct DG classification (i.e., $1 - \varepsilon_d$ in % given by Eq. 1) observed
466 for each building for the EMS-98 damage grade (8a) and the TLS (8b) systems. The x-axis represents
467 the incremental error in the damage grade (e.g., 1 corresponds to the delta of damage grade between
468 observation and prediction, regardless of the DG considered).

469 For the EMS-98 damage scale, correct classification (x-value centred on 0) in the range of 31% to 48%
470 was found, depending on the training/test data sets. The error distribution is quite wide with incorrect
471 predictions of +/-1 DG in the range of +/- 13-35%. Remarkably, when considering the E1 portfolio
472 (Irpinia-1980), for which the post-earthquake inventory was based on another form, as the test set, the
473 error is larger. The predictions at +/-1 DG (i.e., the sum of the x-values Fig. 8a between -1 and +1) were
474 70.5%, 69.9% and 72.8% with portfolios E3, E5 and E7 as the test set, respectively, for an average of
475 71%. For the other portfolios, the average of the predictions at +/- 1 DG was 77%, 78% and 77%,
476 respectively, for portfolios E5, E3 and E7 as the test set. This tendency was also observed for the TLS
477 damage system (Fig. 8b). In this case, the classification of the E1 portfolio was correct on average
478 (average of x-values centred on 0) at 63% and equal to 72%, 73%, and 70.5% for the test on portfolios
479 E5, E3, and E7. For both damage scales, the distributions were skewed, with a larger number of
480 predictions being underestimated (positive x-values), as certainly a consequence of the choice of
481 machine learning models, their implementation (including imbalance issues), the distribution of input
482 and target features considered, or all. The interest of machine learning model is also to have a relevant
483 representation of the errors and limits of these methods.

484

485 **4.3.2. Aggregate-single scenario**

486 Secondly, several aggregated building damage portfolio scenarios were considered to predict a single
487 earthquake, thus testing whether the prediction was improved by increasing the number of post-
488 earthquake damage observations. Three scenarios were tested. They are represented in Fig. 9 applying
489 the EMS-98 damage grade (9a) and the TLS (9b):

490

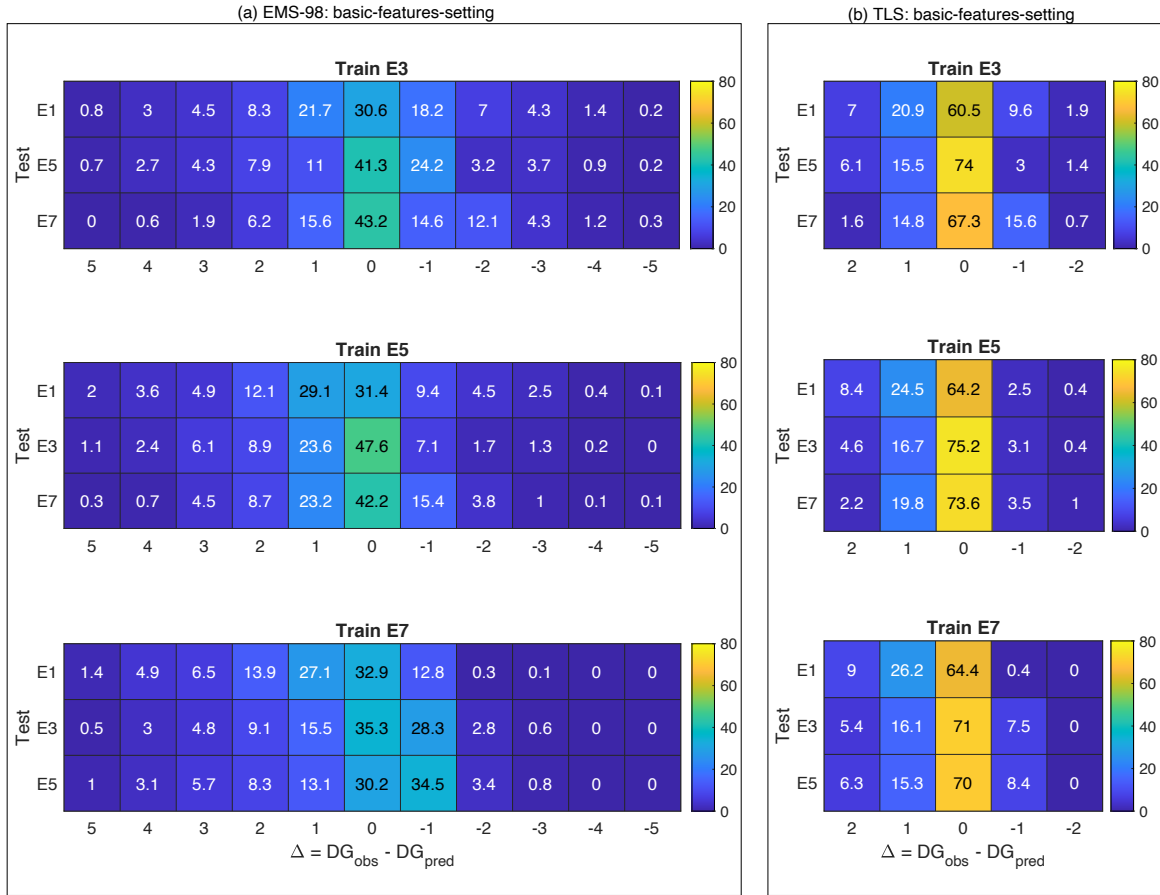
491 (i) Training set: E2+E3+E4+E6 (shown as E2346) – test set: E1, E5 and E7.

492 (ii) Training set: E2+E4+E5+E6 (shown as E2456) – test set: E1, E3 and E7.

493 (iii) Training set: E2+E4+E6+E7 (shown as E2467) – test set: E1, E3 and E5.

494
495
496
497
498
499
500
501
502
503
504
505
506
507
508
509
510
511
512
513
514

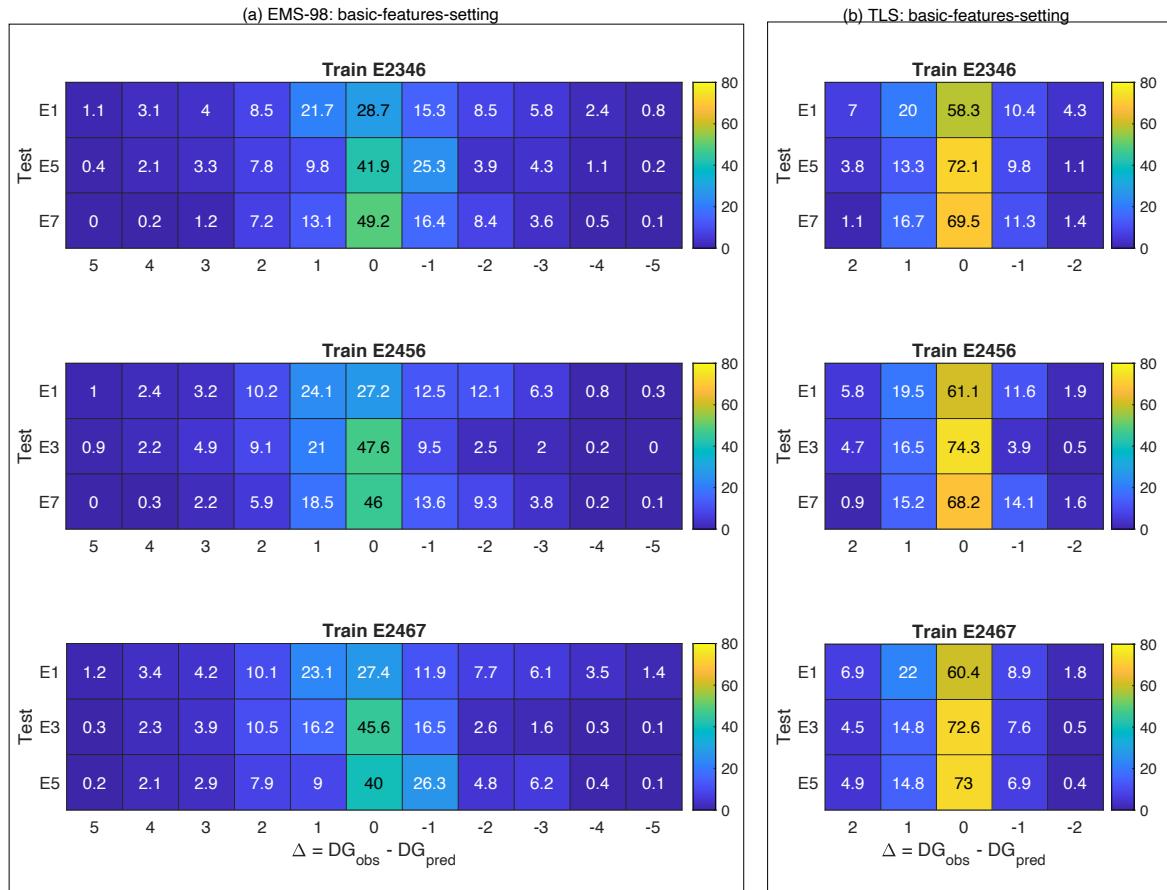
For the EMS-98 damage scale, correct classification (x-value centred on 0) in the range of 27% to 49% was found, depending on the training/test datasets. As in Fig. 8, using the E1 (Irpinia-1980) earthquake for testing scored lower regardless of the portfolio used for training (28.7%, 27.2% and 27.4% prediction accuracy). With E1 as the test set, the predictions at +/-1 DG (i.e., the sum of the x-values on Fig. 9a between -1 and +1) were 65.7%, 63.8% and 62.4% considering the E2346, E2456 and E2467 portfolios as the training set, respectively, for an average of 64% (compared with the 70% score for the single portfolio scenario, Fig. 8a). Other scenarios were also tested by aggregating the building damage portfolios differently (not presented herein), leading to the two main conclusions: (1) the quality and homogeneity of the input data (i.e., building features) affect the efficacy of the heuristic model and (2) this efficacy is limited and not improved by increasing the number of building damage observations, with a score (excluding E1) between 40% and 49% (x-value centred on 0), and up to 78% (average of the two scenarios, Fig. 8a and Fig. 9a) at +/-1 DG. Considering the TLS damage scale (Fig. 9b), a damage prediction efficacy of about 72% was obtained (compared with 72% in Fig. 8b), i.e., but no significant improvement was observed when the number of damaged buildings in the training portfolio was increased. For EMS-98 and TLS, the distributions were skewed, with a larger number of predictions being underestimated (positive x-values). Finally, in conclusion, the heuristic damage assessment model based on the XGBC model gives a better score for TLS damage assessment than for the EMS-98 damage scale. The TLS system also allows for quick assessment of damage on a large scale such as a city or region from an operational point of view.



515

516 **Figure 8.** Distribution of the classification value ($1 - \varepsilon_d$ in % given by Eq. 1) for (a) EMS-98- and (b) TLS-based
 517 damage classification using XGBC machine learning models and considering a single damage portfolio to predict
 518 a single portfolio (single-single scenario). The colour bar indicates the associated value in each cell. The x-values
 519 are the difference between the DG observed and the DG predicted, regardless of the DG considered.

520



521

522 **Figure 9.** Distribution of the classification value ($1 - \varepsilon_d$ in % given by Eq. 1) for (a) EMS-98- and (b) TLS-based
 523 damage classification using XGBC machine learning models and considering an aggregate damage portfolio to
 524 predict a single portfolio (aggregate-single scenario). The colour bar indicates the associated value in each cell.
 525 The x-values are the difference between the DG observed and the DG predicted, regardless of the DG considered.

526

527 4.3.3 Comparing efficacy with the Risk-UE model

528 The efficacy of the heuristic damage assessment model was then compared with conventional damage
 529 prediction methods, i.e., RISK-UE and mean damage relationship (Eq. 2 to 7), considering the basic-
 530 features-settings. For RISK-UE, mean damage μ_d (Eq. 4) was computed using the training set and the
 531 vulnerability index IV for each building (Eq. 5). A vulnerability index was then attributed to all the
 532 buildings in each class defined according to building features. The vulnerability indexes were then
 533 attributed to every building in the test set, mean damage (μ_d) was computed with Eq. 2 and then DG
 534 distribution with Eq. 3, before being compared with the damage portfolio used for testing. Finally, the
 535 distribution of the mean damage observed (Eq. 4) was compared with the distribution of damage directly
 536 on the test set, using Eq. 3.

537 Fig. 10 shows the distribution of absolute errors associated with the RISK-UE, mean damage
 538 relationship, and XGBC methods (with and without compensation for the class-imbalance issue) trained

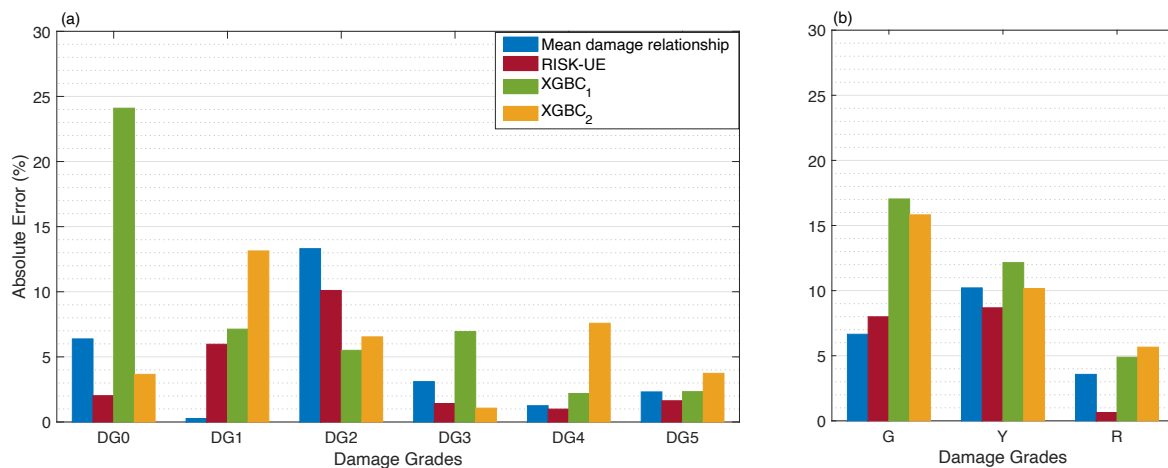
539 on earthquake building damage portfolio E5 and tested on E3. For EMS-98 damage classification (Fig.
 540 10a), the XGBC model (without compensation for class-imbalance issues) resulted in a level of absolute
 541 errors similar to that of the RISK-UE and/or mean damage relationship, except for DG0 (24%). Random
 542 oversampling to compensate for the class-imbalance issues improved the distribution of errors for the
 543 XGBC model (errors less than 8%, except for DG1: 13%).

544 For TLS-based damage classification, the XGBC model also resulted in a similar level of errors
 545 compared with the mean damage relationship and/or RISK-UE methods (Fig. 10b), except for the green
 546 class (no or slight damage, 17.04%). Compensation for class-imbalance issues slightly improved the
 547 distribution of errors for the XGBC model with a 2% drop in errors for green (no/slight damage) and
 548 yellow (moderate damage) classes.

549 Figure 11 shows the distribution of absolute errors trained using the E2456 portfolio and tested on the
 550 E3 portfolio. For EMS-98 damage classification (Fig. 11a), the XGBC model (without compensation
 551 for class-imbalance issues) resulted in a level of errors similar to that of the RISK-UE and/or mean
 552 damage relationship; errors were highest for DG0 with 15.15%. With compensation for the class-
 553 imbalance issues, the XGBC model achieved a slightly lower error distribution for DG0 (5%) and DG3
 554 (4%); however, for other damage grades, the error value increased significantly (DG1: 11%, DG2: 12%
 555 DG4: 7%, DG5: 2%). For TLS-based damage classification, the distribution of absolute errors was
 556 similar for both the XGBC model and the mean damage relationship and/or RISK-UE methods (Fig.
 557 11b). The highest absolute error value was associated with the green (no or slight damage) class of
 558 buildings (16.40%). Compensation for the class-imbalance issues slightly increased the error
 559 distribution for the XGBC model with nearly 5% for buildings in the green (no or slight) and red (heavy)
 560 classes.

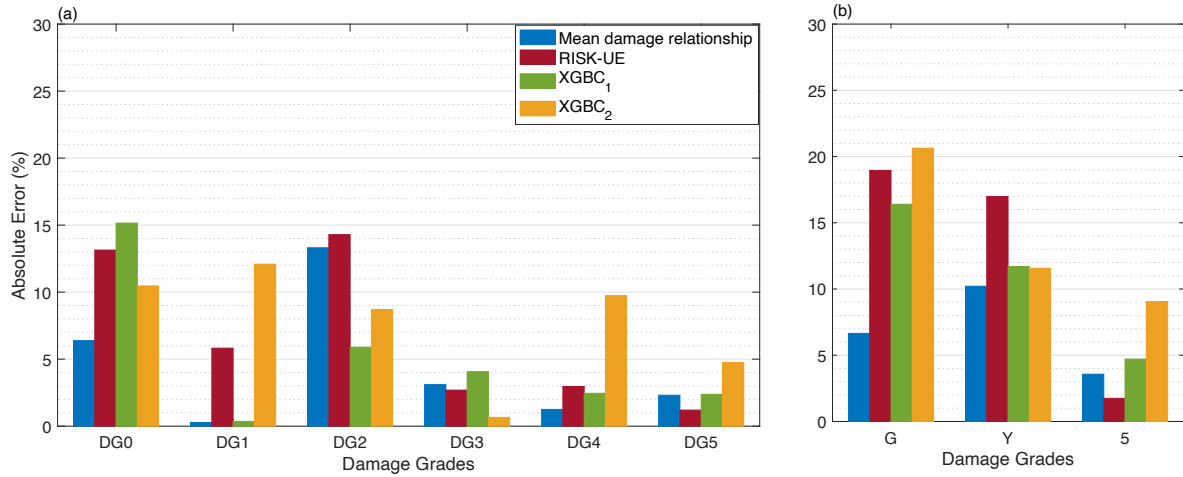
561 These results show that the heuristic building damage model based on the XGBC model, trained using
 562 building damage portfolios with the basic-features-setting, provides a reasonable estimation of potential
 563 damage, particularly with TLS-based damage classification.

564



565

566 **Figure 10.** Comparison of the efficacy of the heuristic model with the conventional model considering the DaDO
567 portfolio (training set: E5; test set: E3) for (a) EMS-98- and (b) TLS-based damage classification. The x-axis is
568 the damage grade and the y-axis is the percentage of absolute error (ϵ_k in % given by Eq. 7). The blue bar
569 corresponds to the mean damage relationship, the red bar corresponds to the RISK-UE method, the green and
570 orange bars correspond to the heuristic model without (XGBC₁) and with (XGBC₂) compensation for the class-
571 imbalance issues, respectively.



572
573 **Figure 11.** Comparison of the efficacy of the heuristic model with the conventional model considering the DaDO
574 portfolio (training set: E2456; test set: E3) for (a) EMS-98- and (b) TLS-based damage classification. The x-axis is
575 the damage grade and the y-axis is the percentage of absolute error (ϵ_k in % given by Eq. 7). The blue bar
576 corresponds to the mean damage relationship, the red bar corresponds to the RISK-UE method, the green and
577 orange bars correspond to the heuristic model without (XGBC₁) and with (XGBC₂) compensation for the class-
578 imbalance issues, respectively.

579

580 5. Discussion

581 Previous studies have aimed to test a machine learning framework for seismic building damage
582 assessment (e.g., Mangalathu et al., 2020; Roeslin et al., 2020; Harirchan et al., 2021; Ghimire et al.,
583 2022). They evaluated various machine learning and data balancing methods to classify earthquake
584 damage to buildings. However, these studies (Mangalathu et al., 2020, Roeslin et al., 2020, Harirchan
585 et al., 2021) had limitations such as limited data samples, damage classes, and building characteristics
586 limited to a spatial coverage and range of seismic demand values. Ghimire et al. (2022) also used a
587 larger building damage database, but did not investigate the importance of input features as a function
588 of damage levels and did not compare machine learning with conventional damage assessment methods.
589 Our study aims to go beyond previous studies by testing advanced machine learning methods and data
590 resampling techniques using the unique DaDO dataset collected from several major earthquakes in Italy.
591 This database covers a wide range of seismic damage and seismic demands of a specific region,
592 including undamaged buildings. Most importantly, this study highlights the importance of input features
593 according to the degrees of damage and finally compares the machine learning models with a classical
594 damage prediction model (Risk-UE). The machine learning models achieved comparable accuracy to

595 the Risk-UE method. In addition, TLS-based damage classification, using red for heavily damaged,
596 yellow for moderate damage, and green for no to slight damage, could be appropriate when the
597 information for undamaged buildings is unavailable during model training.

598 Indeed, it is worth noting that the importance of the input features used in the learning process changes
599 with the degree of damage: this indicates that each feature may have a contribution to the damage that
600 changes with the damage level. Thus, the weight of each feature does not depend linearly on the degree
601 of damage, which is not considered in conventional vulnerability methods.

602 The prediction of seismic damage by machine learning remains until now tested on geographically
603 limited data. The damage distribution is strongly influenced by region-specific factors such as
604 construction quality and regional typologies, implementation of seismic regulations and hazard level.
605 Therefore, machine learning-based models can only work well in regions with comparable
606 characteristics and a host-to-target transfer of these models should be studied. In addition, the
607 distribution of damage is often imbalanced, impacting the performance of machine learning models by
608 assigning higher weights to the features of the majority class. However, data balancing methods like
609 random oversampling can reduce bias caused by imbalanced data during the training phase, but they
610 may also introduce overfitting issues depending on the distribution of input and target features. Thus,
611 integrating data from a wider range of input features and earthquake damage from different regions,
612 relying on a host-to-target strategy, could help achieve a more natural balance of data sets and lead to
613 less biased results. Moreover, the machine learning methods only train on the data available in the
614 learning phase, that reflects the building portfolio in the study area. The importance of the features
615 contributing to the damage could thus be modulated, and would require a host-to-target adjustment for
616 the application of the model to another urban zone/seismic region.”

617 However, the machine learning models trained and tested on the DaDO dataset resulted in similar
618 damage prediction accuracy values reported in existing literature using different models and datasets
619 with different combinations of input features. This might suggest that the uncertainty related to building
620 vulnerability in damage classification may be smaller than the primary source of uncertainty related to
621 the hazard component (such as ground motion, fault rupture, slip duration, etc.).

622

623 In recent years, there has been a proliferation of open building data, such as the OpenStreetMap-based
624 dynamic global exposure model (Schorlemmer et al., 2020) and building damage dataset after an
625 earthquake (such as DaDO). We must therefore continue this paradigm shift initiated by Riedel et al.
626 (2014, 2015) which consisted in identifying the exposure data available and as certain as possible, and
627 in finding the most effective relationships for estimating the damage, unlike conventional approaches
628 which proposed established and robust methods but relying on data not available and therefore difficult
629 to collect. The global dynamic exposure model will make it possible to meet the challenge of modelling
630 exposure on a larger scale on available data, using a tool capable of integrating this large volume of
631 data. Machine learning methods are one such rapidly growing tool that can aid in exposure classification

632 and damage prediction by leveraging readily available information. It is therefore necessary to continue
633 in this direction in order to evaluate the performance of the methods and their pros and cons for
634 maximum efficacy of the prediction of damage.

635 Future works will therefore have to address several key issues that have been discussed here but that
636 need to be further investigated. For example, the weight of the input features varies according to the
637 level of damage, but one can question the systematization of this observation whatever the dataset and
638 the feature considered. The efficiency of the selected models and the management of imbalance data
639 remain to be explored, in particular by verifying regional independence. Taking advantage of the
640 increasing abundance of exposure data and post-seismic observations, the imbalanced feature
641 distribution and observed damage levels could be solved by aggregating datasets independent of the
642 exposure and hazard contexts of the regions, once the host-to-target transfer of the models has been
643 resolved. Finally, key input features (still not yet identified) describing hazard or vulnerability may be
644 unexplored, and incorporating them into the models may improve the accuracy of damage classification.

645

646 **6. Conclusion**

647 In this study, we explored the efficacy of machine learning models trained using DaDO post-earthquake
648 building damage portfolios. We compared six machine learning models: RFC, GBC, XGBC, RFR,
649 GBR, and XGBR. These models were trained on numbers of building features (location, number of
650 storeys, age, floor area, height, position, construction material, regularity, roof type, ground slope
651 condition) and ground motion intensity defined in terms of macro-seismic intensity. The classification
652 models performed slightly better than the regression methods and the XGBC model was ultimately
653 found to be the most efficient model for this dataset. To solve the imbalance issue concerning observed
654 damage, the random oversampling method was applied to the training dataset to improve the efficacy
655 of the heuristic damage assessment model by rectifying the skewed distribution of the target features
656 (DGs).

657 Surprisingly, we found that the weight of the most important building feature evolves according to DG,
658 i.e., the weight of the feature for damage prediction changes depending on the DG considered, which is
659 not taken into account in conventional methods.

660 The basic-features-setting (i.e., considering number of storeys, age, floor area, height and macroseismic
661 intensity, which are accurately evaluated for the existing building portfolio) gave the same accuracy
662 (0.68) as the full-features-settings (0.72) with the TLS-based damage classification method. For training
663 and testing, the homogeneity of the information in the portfolios is a key issue for the definition of a
664 highly effective machine learning model, as shown by the data from the E1 earthquake (Irpinia-1990).
665 However, the efficacy of the model reaches a limit which is not improved by increasing the number of
666 damaged buildings in the portfolio used as the training set, for example. For damage prediction, this
667 type of heuristic model results in approximately 75% correct classification. Other authors (e.g., Riedel

668 et al., 2014, 2015; Ghimire et al. 2022) have already reached this same conclusion by increasing the
669 percentage of the training set compared with the test set.

670 Despite this limit threshold, the level of accuracy achieved remains similar to that attained by
671 conventional methods, such as Risk-UE and the mean damage relationship, for the basic-features-
672 settings and TLS-based damage classification (error values less than 17 %). Machine learning models
673 trained on post-earthquake building damage portfolios could provide a reasonable estimation of damage
674 for a different region with similar building portfolios, after host-to-target adjustment.

675 Some variability may have been introduced into the damage prediction model due to the framework
676 defined to translate the original damage scale to the EMS-98 damage scale and because in the DaDO
677 database, the year of construction and the floor area of each building are provided as interval values,
678 and missing locations of buildings were replaced with the location of local administrative centres. The
679 latter can lead to a smoothing of the macro-seismic intensities to be considered for each structure and
680 also affect the distance to the earthquake. Similarly, the building damage surveys were carried out after
681 the seismic sequence, which includes aftershocks as well as the mainshock, whereas the MSI input
682 corresponds to the mainshock from the USGS ShakeMap. All these issues may reduce the efficacy of
683 the heuristic model and its limit threshold. Addressing these issues could improve the damage prediction
684 performance of machine learning models.

685

686 **Code availability**

687 The machine learning models were developed using Scikit-learn documentation and the value of
688 hyperparameters used are provided in table 3.

689 **Data availability**

690 The data used in this study is available in the Database of Observed Damage (DaDO) web-GIS platform
691 of the Civil Protection Department, developed by the Eucentre Foundation.

692 https://egeos.eucentre.it/danno_osservato/web/danno_osservato?lang=EN.

693

694 **Author contribution**

695 Subash Ghimire: Conceptualization, methodology, data preparation, investigation, visualization, draft
696 preparation. Philippe Guéguen: Conceptualization, investigation, visualization, supervision, review and
697 editing. Adrien Pothon: Conceptualization, supervision, review and editing draft. Danijel Schorlemmer:
698 Conceptualization, supervision, review and editing draft.

699

700 **Competing interests**

701 The authors declare that they have no conflict of interest.

702

703 **Acknowledgment**

704 The author(s) disclosed receipt of the following financial support for the research, authorship, and/ or
705 publication of this article: This study was funded by the URBASIS-EU project (H2020-MSCA- ITN-
706 2018, Grant No. 813137). A.P. and P.G. thank the AXA Research Fund supporting the project New
707 Probabilistic Assessment of Seismic Hazard, Losses and Risks in Strong Seismic Prone Regions. P.G.
708 thanks LabEx OSUG@2020 (Investissements d’avenir- ANR10LABX56)

References

- 709 ATC: ATC-20-1, Field Manual: Postearthquake Safety Evaluation of Buildings Second Edition,,
710 Applied Technology Council, Redwood City, California., 2005.
- 711 Azimi, M., Eslamlou, A. D., and Pekcan, G.: Data-driven structural health monitoring and damage
712 detection through deep learning: State-ofthe- art review, <https://doi.org/10.3390/s20102778>, 2020.
- 713 Baggio, C., Bernardini, A., Colozza, R., Pinto, A. V, and Taucer, F.: Field Manual for post-earthquake
714 damage and safety assessment and short term countermeasures (AeDES) Translation from Italian:
715 Maria ROTA and Agostino GORETTI, 2007.
- 716 Bazzurro, P., Cornell, C. A., Menun, C., and Motahari, M.: GUIDELINES FOR SEISMIC
717 ASSESSMENT OF DAMAGED BUILDINGS, in: 13th World Conference on Earthquake Engineering,
718 Vancouver, B.C. m Canada, 74–76, <https://doi.org/10.5459/bnzsee.38.1.41-49>, 2004.
- 719 Branco, P., Ribeiro, R. P., Torgo, L., Krawczyk, B., and Moniz, N.: SMOGN: a Pre-processing
720 Approach for Imbalanced Regression, *Proc. Mach. Learn. Res.*, 74, 36–50, 2017.
- 721 Breiman, L.: Random Forests, *Mach. Learn.*, 5–32, 2001.
- 722 Chen, T. and Guestrin, C.: XGBoost: A Scalable Tree Boosting System, in: 22nd acm sigkdd
723 international conference on knowledge discovery and data mining, 785–794,
724 <https://doi.org/10.1145/2939672.2939785>, 2016.
- 725 Daniell, J. E., Schaefer, A. M., Wenzel, F., and Tsang, H. H.: The global role of earthquake fatalities in
726 decision-making: earthquakes versus other causes of fatalities, *Proc. Sixt. world Conf. Earthq. Eng.*
727 *Santiago, Chile*, 9–13, 2017.
- 728 Dolce, M., Speranza, E., Giordano, F., Borzi, B., Bocchi, F., Conte, C., Meo, A. Di, Faravelli, M., and
729 Pascale, V.: Observed damage database of past italian earthquakes: The da.D.O. WebGIS, *Boll. di*
730 *Geofis. Teor. ed Appl.*, 60, 141–164, <https://doi.org/10.4430/bgta0254>, 2019.
- 731 Estabrooks, A. and Japkowicz, N.: A mixture-of-experts framework for learning from imbalanced data
732 sets, *Lect. Notes Comput. Sci.* (including Subser. *Lect. Notes Artif. Intell. Lect. Notes Bioinformatics*),
733 2189, 34–43, https://doi.org/10.1007/3-540-44816-0_4, 2001.
- 734 FEMA: Hazus –MH 2.1 Multi-hazard Loss Estimation Methodology Earthquake, 2003.
- 735 Friedman, J. H.: *Greedy Function Approximation: A Gradient Boosting Machine*, 1999.
- 736 Del Gaudio, C., Scala, S. A., Ricci, P., and Verderame, G. M.: Evolution of the seismic vulnerability of
737 masonry buildings based on the damage data from L’Aquila 2009 event, *Bull. Earthq. Eng.*, 19,
738 <https://doi.org/10.1007/s10518-021-01132-x>, 2021.
- 739 Ghimire, S., Guéguen, P., Giffard-Roisin, S., and Schorlemmer, D.: Testing machine learning models
740 for seismic damage prediction at a regional scale using building-damage dataset compiled after the 2015

- 741 Gorkha Nepal earthquake, *Earthq. Spectra*, <https://doi.org/10.1177/87552930221106495>, 2022.
- 742 Grünthal, G.: Escala Macro Sísmica Europea EMS - 98, 101 pp., 1998.
- 743 Guéguen, P., Michel, C., and Lecorre, L.: A simplified approach for vulnerability assessment in
744 moderate-to-low seismic hazard regions: Application to Grenoble (France), *Bull. Earthq. Eng.*, 5, 467–
745 490, <https://doi.org/10.1007/s10518-007-9036-3>, 2007.
- 746 Guettiche, A., Guéguen, P., and Mimoune, M.: Seismic vulnerability assessment using association rule
747 learning: application to the city of Constantine, Algeria, *Nat. Hazards*, 86, 1223–1245,
748 <https://doi.org/10.1007/s11069-016-2739-5>, 2017.
- 749 Harirchian, E., Kumari, V., Jadhav, K., Rasulzade, S., Lahmer, T., and Das, R. R.: A synthesized study
750 based on machine learning approaches for rapid classifying earthquake damage grades to rc buildings,
751 *Appl. Sci.*, 11, <https://doi.org/10.3390/app11167540>, 2021.
- 752 Hegde, J. and Rokseth, B.: Applications of machine learning methods for engineering risk assessment
753 – A review, *Saf. Sci.*, 122, 104492, <https://doi.org/10.1016/j.ssci.2019.09.015>, 2020.
- 754 Japkowicz, N. and Stephen, S.: The class imbalance problem A systematic study *fulltext.pdf*, 6, 429–
755 449, 2002.
- 756 Kim, T., Song, J., and Kwon, O. S.: Pre- and post-earthquake regional loss assessment using deep
757 learning, *Earthq. Eng. Struct. Dyn.*, 49, 657–678, <https://doi.org/10.1002/eqe.3258>, 2020.
- 758 Lagomarsino, S. and Giovinazzi, S.: Macroseismic and mechanical models for the vulnerability and
759 damage assessment of current buildings, *Bull. Earthq. Eng.*, 4, 415–443,
760 <https://doi.org/10.1007/s10518-006-9024-z>, 2006.
- 761 Lagomarsino, S., Cattari, S., and Ottonelli, D.: The heuristic vulnerability model: fragility curves for
762 masonry buildings, Springer Netherlands, 3129–3163 pp., <https://doi.org/10.1007/s10518-021-01063-7>, 2021.
- 764 Lundberg, S. M. and Lee, S.-I.: A Unified Approach to Interpreting Model Predictions, in: 31st
765 Conference on Neural Information Processing Systems, 2017.
- 766 Mangalathu, S. and Jeon, J.-S.: Regional Seismic Risk Assessment of Infrastructure Systems through
767 Machine Learning: Active Learning Approach, *J. Struct. Eng.*, 146, 04020269,
768 [https://doi.org/10.1061/\(asce\)st.1943-541x.0002831](https://doi.org/10.1061/(asce)st.1943-541x.0002831), 2020.
- 769 Mangalathu, S., Sun, H., Nweke, C. C., Yi, Z., and Burton, H. V.: Classifying earthquake damage to
770 buildings using machine learning, *Earthq. Spectra*, 36, 183–208,
771 <https://doi.org/10.1177/8755293019878137>, 2020.
- 772 Milutinovic, Z. and Trendafiloski, G.: Risk-UE An advanced approach to earthquake risk scenarios with
773 applications to different european towns, Rep. to WP4 vulnerability Curr. Build., 1–83, 2003.
- 774 MINVU: Ministry of Housing and Urbanism of Chile, Terremoto y Tsunami 27F, 2010.
- 775 Morfidis, K. and Kostinakis, K.: Approaches to the rapid seismic damage prediction of r/c buildings
776 using artificial neural networks, *Eng. Struct.*, 165, 120–141,
777 <https://doi.org/10.1016/j.engstruct.2018.03.028>, 2018.
- 778 Mouroux, P. and Le Brun, B.: Presentation of RISK-UE Project, *Bull. Earthq. Eng.* 2006 44, 4, 323–
779 339, <https://doi.org/10.1007/S10518-006-9020-3>, 2006.

- 780 MTPTC: Ministère des Travaux Publics, Transports et Communications: Evaluation des Bâtiments:
781 https://www.mtptc.gouv.ht/accueil/recherche/article_7.html, 2010.
- 782 NPA: Police Countermeasures and Damage Situation associated with 2011Tohoku district - off the
783 Pacific Ocean Earthquake Total burn down Inundated below floor level Partially damaged Property
784 damages Damaged roads Partial burn down March 10, 2021,
785 https://doi.org/https://www.npa.go.jp/news/other/earthquake2011/pdf/higaijokyo_e.pdf (last access: 22
786 March 2021), 2021.
- 787 NPC: Nepal Planning Commission (NPC). 2015 Nepal Earthquake: Open Data Portal:
788 </eq2015.npc.gov.np/#/>, (last access: 22 March 2021), 2015.
- 789 Pedregosa, F., Varoquaux, G., Buitinck, L., Louppe, G., Grisel, O., and Mueller, A.: Scikit-learn,
790 *GetMobile Mob. Comput. Commun.*, 19, 29–33, <https://doi.org/10.1145/2786984.2786995>, 2011.
- 791 Riedel, I., Guéguen, P., Dunand, F., and Cottaz, S.: Macroscale vulnerability assessment of cities using
792 association rule learning, *Seismol. Res. Lett.*, 85, 295–305, <https://doi.org/10.1785/0220130148>, 2014.
- 793 Riedel, I., Guéguen, P., Dalla Mura, M., Pathier, E., Leduc, T., and Chanussot, J.: Seismic vulnerability
794 assessment of urban environments in moderate-to-low seismic hazard regions using association rule
795 learning and support vector machine methods, *Nat. Hazards*, 76, 1111–1141,
796 <https://doi.org/10.1007/s11069-014-1538-0>, 2015.
- 797 Roeslin, S., Ma, Q., Juárez-García, H., Gómez-Bernal, A., Wicker, J., and Wotherspoon, L.: A machine
798 learning damage prediction model for the 2017 Puebla-Morelos, Mexico, earthquake, *Earthq. Spectra*,
799 36, 314–339, <https://doi.org/10.1177/8755293020936714>, 2020.
- 800 Salehi, H. and Burgueño, R.: Emerging artificial intelligence methods in structural engineering, *Eng.*
801 *Struct.*, 171, 170–189, <https://doi.org/10.1016/j.engstruct.2018.05.084>, 2018.
- 802 Scala, S. A., Del Gaudio, C., and Verderame, G. M.: Influence of construction age on seismic
803 vulnerability of masonry buildings damaged after 2009 L’Aquila earthquake, *Soil Dyn. Earthq. Eng.*,
804 157, 107199, <https://doi.org/10.1016/J.SOILDYN.2022.107199>, 2022.
- 805 Schorlemmer, D., Beutin, T., Cotton, F., Garcia Ospina, N., Hirata, N., Ma, K. F., ... and Wyss, M. :
806 Global dynamic exposure and the OpenBuildingMap-a big-data and crowd-sourcing approach to
807 exposure modeling, In *EGU General Assembly Conference Abstracts* (p. 18920), 2020.
- 808 Seo, J., Dueñas-Osorio, L., Craig, J. I., and Goodno, B. J.: Metamodel-based regional vulnerability
809 estimate of irregular steel moment-frame structures subjected to earthquake events, *Eng. Struct.*, 45,
810 585–597, <https://doi.org/10.1016/j.engstruct.2012.07.003>, 2012.
- 811 Silva, V., Crowley, H., Pagani, M., Monelli, D., and Pinho, R.: Development of the OpenQuake engine,
812 the Global Earthquake Model’s open-source software for seismic risk assessment, *Nat. Hazards*, 72,
813 1409–1427, <https://doi.org/10.1007/s11069-013-0618-x>, 2014.
- 814 Silva, V., Pagani, M., Schneider, J., and Henshaw, P.: Assessing Seismic Hazard and Risk Globally for
815 an Earthquake Resilient World, *Contrib. Pap. to GAR 2019*, 24 p., 2019.
- 816 Stojadinović, Z., Kovačević, M., Marinković, D., and Stojadinović, B.: Rapid earthquake loss
817 assessment based on machine learning and representative sampling, *Earthq. Spectra*,
818 <https://doi.org/10.1177/87552930211042393>, 2021.
- 819 Sun, H., Burton, H. V., and Huang, H.: Machine learning applications for building structural design and
820 performance assessment: State-of-the-art review, *J. Build. Eng.*, 33, 101816,

- 821 <https://doi.org/10.1016/j.jobe.2020.101816>, 2021.
- 822 Wald, D. J., Worden, B. C., Quitoriano, V., and Pankow, K. L.: ShakeMap manual: technical manual,
823 user's guide, and software guide, Techniques and Methods, <https://doi.org/10.3133/tm12A1>, 2005.
- 824 Wang, C., Yu, Q., Law, K. H., McKenna, F., Yu, S. X., Taciroglu, E., Zsarnóczay, A., Elhaddad, W.,
825 and Cetiner, B.: Machine learning-based regional scale intelligent modeling of building information for
826 natural hazard risk management, Autom. Constr., 122, <https://doi.org/10.1016/j.autcon.2020.103474>,
827 2021.
- 828 Xie, Y., Ebad Sichani, M., Padgett, J. E., and DesRoches, R.: The promise of implementing machine
829 learning in earthquake engineering: A state-of-the-art review, Earthq. Spectra,
830 <https://doi.org/10.1177/8755293020919419>, 2020.
- 831 Xu, Y., Lu, X., Cetiner, B., and Taciroglu, E.: Real-time regional seismic damage assessment
832 framework based on long short-term memory neural network, Comput. Civ. Infrastruct. Eng., 1–18,
833 <https://doi.org/10.1111/mice.12628>, 2020a.
- 834 Xu, Z., Wu, Y., Qi, M. zhu, Zheng, M., Xiong, C., and Lu, X.: Prediction of structural type for city-
835 scale seismic damage simulation based on machine learning, Appl. Sci., 10,
836 <https://doi.org/10.3390/app10051795>, 2020b.
- 837